

# Entanglement Classification from a Topological Perspective

Dmitry Melnikov

*International Institute of Physics, Federal University of Rio Grande do Norte,  
Campus Universitário, Lagoa Nova, Natal-RN 59078-970, Brazil*

## Abstract

Classification of entanglement is an important problem in Quantum Resource Theory. In this paper I discuss an embedding of this problem in the context of Topological Quantum Field Theories (TQFT). This approach allows classifying entanglement patterns in terms of topological equivalence classes. In the bipartite case a classification equivalent to the one by Stochastic Local Operations and Classical Communication (SLOCC) is constructed by restricting to a simple class of connectivity diagrams. Such diagrams characterize quantum states of TQFT up to braiding and tangling of the “connectome”. In the multipartite case the same restricted topological classification only captures a part of the SLOCC classes, in particular, it does not see the W entanglement of three qubits. Non-local braiding of connections may solve the problem, but no finite classification is attempted in this case. Despite incompleteness, the connectome classification has a straightforward generalization to any number and dimension of parties and has a very intuitive interpretation, which might be useful for understanding specific properties of entanglement and for design of new quantum resources.

## 1 Introduction

The term entanglement in reference to intricate correlations existing between parts of a quantum system raises natural analogies with topology. An early discussion of this observation appears in [1], for example. Specifically, knot theory is a branch of topology that studies classical entanglement of one-dimensional objects, such as curves, ropes or ribbons, and the question is whether analogy between this classical entanglement and quantum correlations has any strict mathematical meaning, or whether there is any practical use of it for quantum physics.

Topological quantum field theories (TQFTs) [2, 3] offer an obvious setup to address such questions. These theories appeared as a link connecting knot theory and quantum mechanics (quantum field theory), endowing knots and links with a notion of quantum correlators [4]. In the instances of quantum mechanics appearing in the context of TQFT all observables are expressed in terms of the topological invariants of knots, and so must do the entanglement and its measures. The question asked in [1] is more specific: whether the character of quantum entanglement is encoded in the linking patterns of knots. This question can be motivated by the classification problems in knots and in quantum information theory. On one hand, classification and counting of knots is a fundamental problem of knot theory. On the other, one is interested in understanding possible patterns of entanglement. The latter is an important problem of Quantum Resource Theory: the structure of the state’s entanglement defines quantum tasks, for which this state is a suitable resource.

Further motivation stems from the fact that physical systems governed by TQFTs, such as two-dimensional electrons in strong magnetic fields, or concept condensed matter systems with Majorana

fermions, can serve a basis for a quantum computer, whose states are naturally robust against decoherence [5–7]. From the theoretical point of view, the most natural set of basic operations (gates) in such a computer is provided by braiding of the quasiparticles in the above systems – a procedure of creating knots (links) from the particles’ worldlines. Then the question of [1] becomes a question of vocabulary, translation of known quantum algorithms into the language of mathematics of knot theory.

Different aspects of topological quantum computation and physical realizations of topological phases of matter have been by now extensively addressed in the literature. The canonical reference for this subject is the review [8]. In the present note I would like to take a step back towards the original question and discuss the problem of quantum entanglement classification from the point of view of formal TQFT. A systematic early effort to discuss the entanglement features of knots and to build the knot theory version of the quantum computer based on the ideas similar to the ones in [1] was taken in the following (likely incomplete) set of references: [9–16]. (See a review of these results and further references in [17].)

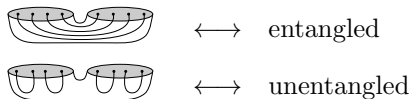
The purpose of this paper is to discuss what knots or rather TQFTs teach us about quantum entanglement, or how they encode the entanglement and how they classify its different types. Besides [1], this expands and complements similar recent studies, e.g. [18–29]. Here I will start from the axiomatic approach to TQFT, as in [24], and compare different forms of entanglement suggested by topology to the Quantum Resource Theory classification based on Stochastic Local Operations and Classical Communication (SLOCC). The topologies surging in the present approach will be different from that of [20], for example, in that they will be based on tangles (open lines), rather than links (closed lines).

Axiomatic TQFT associates a quantum state to a topological space with a boundary (see [17, 24] for a minimal review of the axioms and definitions). The boundary defines the Hilbert space the state belongs to, while the bulk – the details of the state in this Hilbert space. Different spaces can be glued along equivalent boundaries to realize scalar products, matrix multiplication, or more general tensor contractions. An important realization of the TQFT axioms is provided by functional integrals of metric independent action functionals (partition functions).

Topological spaces are equivalent up to homeomorphisms. In comparison to metric spaces (non-topological partition functions) they already define classes of equivalence of quantum states. Bulk-disconnected boundaries correspond to product states. Disconnected boundary components introduce the notion of locality. All this sets a stage for the discussion of entanglement and its classification.

The naive classification by topology in a generic TQFT gives an infinite number of topological classes. However, for specific CFT’s with finite-dimensional Hilbert spaces like the Chern-Simons theory, there are linear relations between states of different topology and the number of classes is finite. Yet, relations make the classification problem more complicated. Instead, in this note I consider a simpler classification based on locality and connectivity, and relate it to the SLOCC one. In the case of boundaries being 2-spheres with punctures (in  $SU(2)_k$  Chern-Simons) the classification reduces to connectivity diagrams (adjacency matrices with additional equivalence relation due to locality).

The connectivity diagram classification works in the simplest case of the pair of qubits:



Shaded discs in these heuristic diagrams represent boundary spheres  $S^2$  and lines – evolution of punctures in the bulk (Wilson lines). I argue that these are the only relevant ways to connect the punctures up to local braiding and tangling. Further details of the identification are provided in the body of the paper.

Simple connectivity classification does not generalize to the case of generic qudits in a straightforward way. The main problem is that the dimension of the Hilbert space grows too fast with the number of additional Wilson lines. One needs to project these large Hilbert spaces onto appropriate subspaces. Necessary projectors exist in TQFT, known as Jones-Wenzl projectors [30, 31]. They allow building a connectivity classification matching the SLOCC one in the bipartite case. This result is a consequence

of the fact that the bipartite SLOCC classification is related to a simple property of reduced density matrices and can be reproduced in terms of highest weight vectors of irreducible representation of  $SU(2)$ , to which the Jones-Wenzl projectors have a direct relation.

Generalization of the SLOCC classification to a higher number of parties faces certain challenges. It is understood that the tripartite case of qubits has four nonequivalent classes [32], while for four [33] and more parties the SLOCC classification is only partially successful [34]. The multipartite entanglement classes are determined up to a number of parameters not fixed by the SLOCC. In other words, the precise classification gives an infinite number of entanglement classes, making the full version impractical and requiring some coarsening.

This is precisely the situation with the topological classification, which a priori predicts an infinite number of classes. This work provides an attempt to build such a coarsening. It turns out that the extension of the above approach to three and more qubits is not able to capture all the SLOCC classes. For three qubits the connectivity diagrams reproduce only three out of four classes. The most intricate  $W$  class is not captured by the connectivity, but can rather be achieved through non-local braiding. Despite this drawback, the connectivity classification has important advantages, because it makes apparent and intuitive many properties of entanglement and its generalization to any number and dimension of the parties.

The results of the topological classification can be compared with other examples of coarse classifications, such as [35]. The latter work associates different forms of entanglement with different geometrical, rather than topological forms, the polytopes, which appear as spaces characterizing irreducible action of SLOCC operators on local density matrices. The polytope classification detects the  $W$  class in the 3-qubit case, and considerably more classes of genuine 4-qubit entanglement (seven versus two) as compared to the connectivity classification. An advantage of the latter is that the entanglement information is represented by the state itself, which is important for entanglement engineering.

The remainder of this paper is organized as follows. In section 2 I review a connection of the classification of the bipartite entanglement with the representation theory and highest weight vectors of irreducible representations. In section 3 the topological entanglement is discussed as the avatar of the quantum one. Salient aspects of TQFT of dimensions one, two and three is discussed in that section as well as the setup of the entanglement classification in such theories. In the following part of the paper I focus on the case of boundaries being 2-spheres with punctures and introduce a minimal classification in terms of connectivity diagrams. Since the simple connectivity classification does not properly capture the classes of bipartite entanglement for generic qudits, in section 4 I elaborate it by introducing necessary projectors. In section 5 I discuss the classification of the 3-partite entanglement and the fate of the  $W$ -type entanglement in the topological classification. I summarize the results of the paper in section 6.

## 2 Entanglement and representation theory

Before discussing the topological interpretation of entanglement let us first review the connection of the latter with representations of unitary groups. I will illustrate it by the example of  $SU(2)$  and focus on the bipartite entanglement. Further details and generalizations can be found elsewhere. See [35] for alternative ways of classifying entanglement via irreducible representations.

For  $SU(2)$ , a qubit is realized by the fundamental representation of the group. In the case of a pair of qubits the states are decomposed into a pair of irreducible representations  $\mathbf{1}$  and  $\mathbf{3}$ :

$$\begin{aligned} \mathbf{1} : & \quad \frac{1}{\sqrt{2}} (|01\rangle - |10\rangle) \\ \mathbf{3} : & \quad |00\rangle \quad \frac{1}{\sqrt{2}} (|01\rangle + |10\rangle) \quad |11\rangle \end{aligned} \tag{1}$$

Highest weight vectors of the two representations correspond to two classes of SLOCC entanglement (Bell and separable).



is entangled is to compute the von Neumann entropy. The reduced density matrices of the subsystem  $A$  for the two states are

$$\rho_1(A) = \left[ \text{diagram of a sphere} \right]^{-1} \begin{array}{c} \Sigma_A \\ \Sigma_A \end{array} \quad \text{or} \quad \rho_2(A) = \left[ \text{diagram of a cylinder} \right]^{-1} \begin{array}{c} \Sigma_A \\ \Sigma_A \end{array}. \quad (6)$$

The diagrams in the square brackets are the normalization factors (closed manifolds without boundary correspond to  $\mathbb{C}$ -numbers in the axiomatic TQFT). The von Neumann entropy  $S_E = -\text{tr} \rho_A \log \rho_A$  can be computed using the replica trick. It is not hard to show [24, 36] that for the first state  $S_E = 0$ , while for the “entangled” one it is

$$S_E(A) = \log \left[ \text{diagram of a cylinder with a handle} \right] = \log \dim \mathcal{H}_{\Sigma_A}. \quad (7)$$

If in state (5) the two boundaries  $\Sigma_A$  and  $\Sigma_B$  are homeomorphic and connected by a cobordism of the simplest topology (simply connected) then one can understand the reduced density matrix, the cylinder in (3), as an identity operator, so the von Neumann entropy is just the logarithm of the trace of the identity over the Hilbert subspace  $\mathcal{H}_A$ . The latter equals  $\dim \mathcal{H}_A$ , which means that (5) is maximally entangled.

One can also consider cobordisms of different topology and multipartite systems, as in the following example,



A natural question in this case is about the relation between different topologies associated to the states and equivalence classes under the action of SLOCC. Indeed, topology provides a classification of quantum states, identifying states that are homeomorphic. In the finite-dimensional realizations of TQFT there are even stronger relations leading to a discrete and finite classification. So, is there any relation between the SLOCC classification and the topological one?

Let us first review TQFTs in low dimensions. In the three-dimensional case we will discuss a specific identification proposal.

**One-dimensional TQFT.** In one-dimensional TQFT one has a set of points and lines connecting the points. Points are boundaries of lines and for each line one needs a pair of points, so the number of points must be even. Hilbert spaces can be associated to pairs of points, the pairs should not necessarily be equivalent. It is clear that a single pair of points may represent only a one-dimensional Hilbert space, so the minimal non-trivial case is achieved with two pairs. The total Hilbert space is then obtained by tensoring the individual Hilbert spaces.

The simplest example can be obtained from four pairs of points divided into two equal subsystems. Then one can have the following states:

$$\begin{array}{c} \text{---} \\ \text{---} \end{array} \begin{array}{c} \text{---} \\ \text{---} \end{array}, \quad \begin{array}{c} \text{---} \\ \text{---} \end{array} \begin{array}{c} \text{---} \\ \text{---} \end{array}, \quad \text{and} \quad \begin{array}{c} \text{---} \\ \text{---} \\ \text{---} \\ \text{---} \end{array}, \quad (9)$$

up to local operations of permutation within left and right subsystems, cf. (4) and (5). Since we expect that classes of entanglement are independent from local unitary operations on the parties, such as local permutations, the above diagrams exhaust all the possibilities. In fact, the first and the second states

in (9) are equivalent. This is a consequence of the triviality of the Hilbert space of a pair of lines and can be seen directly if one uses the natural basis of the 4-point Hilbert space:

$$|e_1\rangle = \begin{array}{c} \text{---} \\ \text{---} \\ \text{---} \end{array} , \quad |e_2\rangle = \begin{array}{c} \text{---} \\ \text{---} \\ \text{---} \end{array} . \quad (10)$$

This is not an orthonormal basis, but it can be used to construct one

$$|0\rangle = \frac{1}{\bigcirc} |e_1\rangle, \quad |1\rangle = \frac{1}{\sqrt{(\bigcirc)^2 - 1}} \left( |e_2\rangle - \frac{1}{\bigcirc} |e_1\rangle \right). \quad (11)$$

As above, the circle  $\bigcirc$  is a number associated to a closed manifold in the given one-dimensional TQFT.

Note that apart from states (11) one can also consider the option

$$|e_3\rangle = \begin{array}{c} \text{---} \\ \text{---} \\ \text{---} \end{array} . \quad (12)$$

Since we consider a one-dimensional theory, the details of the crossing are not important, it should only reflect a permutation of two points. As a true permutation, such operation must be idempotent. We can use the above vector to define a new normalized basis vector

$$|2\rangle = \sqrt{\frac{\bigcirc + 1}{\bigcirc (\bigcirc - 1)(\bigcirc + 2)}} \left( |e_3\rangle - |0\rangle - \frac{\bigcirc - 1}{\sqrt{(\bigcirc)^2 - 1}} |1\rangle \right), \quad (13)$$

orthogonal to  $|0\rangle$  and  $|1\rangle$ .

One can check that the first two states in (9) are annihilated by either projectors  $|1\rangle\langle 1|$  or  $|2\rangle\langle 2|$  applied one the left or on the right state. More generally, if any two parties are connected by only a pair of lines, they are essentially disconnected,

$$\begin{array}{c} \bullet \\ \text{---} \\ \bullet \end{array} \sim \begin{array}{c} \bullet \\ \text{---} \\ \bullet \end{array} \quad (14)$$

With respect to the three-dimensional Hilbert space with the basis (11) and (13), the first two states in (9) correspond to matrices of rank one, while the last state – to a matrix of rank three. The problem now is that there seem to be no diagrammatic representation for a state of rank two. Note that adding crossings to the diagrams in (9) does not change anything, since the crossings can be undone by local permutations on the left and right states.

The problem can be solved if we project out the subspace generated by vector  $|2\rangle$ . There are few additional reasons for doing this. Below we will embed the one-dimensional TQFTs in the three-dimensional ones. In common choices of three-dimensional TQFTs, vector  $|2\rangle$  is linearly-dependent of  $|0\rangle$  and  $|1\rangle$  through the so-called skein-relations. Such linear dependence happens naturally in the one-dimensional case if one chooses  $\bigcirc = 2$ . In the latter case vector  $|2\rangle$  is null.

If we focus on the TQFTs with skein relations, that is linear dependence of the diagrams with crossings of the diagrams without crossings, then the case of a pair of quadruple of points illustrates the situation of a pair of qubits with entanglement types characterized by diagrams

$$\begin{array}{c} \text{---} \\ \text{---} \\ \text{---} \\ \text{---} \end{array} , \quad \text{and} \quad \begin{array}{c} \text{---} \\ \text{---} \\ \text{---} \\ \text{---} \end{array} , \quad (15)$$

corresponding to the separable and Bell classes of SLOCC respectively. The Schmidt decomposition of the above in the basis (11) has one and two terms respectively. Therefore, with a bit of redundancy due to some additional constraints (here triviality of the Hilbert space associated with two points), topological (connectivity) diagrams characterize the main entanglement patterns of a pair of qubits.

Next we must consider higher dimensional Hilbert spaces in bipartite systems. If we consider the Hilbert space of six points then one has the following types of connectivity diagrams,

$$\begin{array}{cccc} \begin{array}{c} \text{---} \\ \text{---} \\ \text{---} \\ \text{---} \end{array} & , & \begin{array}{c} \text{---} \\ \text{---} \\ \text{---} \\ \text{---} \\ \text{---} \end{array} & , & \begin{array}{c} \text{---} \\ \text{---} \\ \text{---} \\ \text{---} \\ \text{---} \\ \text{---} \end{array} & , & \text{and} & \begin{array}{c} \text{---} \\ \text{---} \\ \text{---} \\ \text{---} \\ \text{---} \\ \text{---} \end{array} . \end{array} \quad (16)$$

Again, the first two diagrams are equivalent, so there are three independent classes of states up to local operations. The diagrams then correspond to matrices of rank one, two and to a matrix of the maximal rank. If the dimension of the associated Hilbert space (maximal rank) were three then we would be dealing with the case of a pair of qutrits. However, this is not the case if define the Hilbert space as before. There are five crossing-free diagrams to make the basis:

$$|e_1\rangle = \begin{array}{c} \text{---} \\ \text{---} \\ \text{---} \\ \text{---} \end{array} , \quad |e_2\rangle = \begin{array}{c} \text{---} \\ \text{---} \\ \text{---} \\ \text{---} \\ \text{---} \end{array} , \quad |e_3\rangle = \begin{array}{c} \text{---} \\ \text{---} \\ \text{---} \\ \text{---} \\ \text{---} \\ \text{---} \end{array} , \quad |e_4\rangle = \begin{array}{c} \text{---} \\ \text{---} \\ \text{---} \\ \text{---} \\ \text{---} \\ \text{---} \\ \text{---} \end{array} , \quad |e_5\rangle = \begin{array}{c} \text{---} \\ \text{---} \end{array} . \quad (17)$$

In general  $2n$ -point Hilbert has a basis labeled by the elements of Temperley-Lieb algebra  $TL_n$ .

For the five-dimensional Hilbert space of (17) the diagrams of (16) are not enough to capture all the types of the SLOCC entanglement. In particular, they miss the rank three and rank four cases. It is obvious that the situation is even worse for higher dimensional Hilbert spaces, since the number of connectivity diagrams grows linearly with the number of points, while the dimension of the Hilbert space – exponentially.

In section 4 we will solve the mismatch problem by building a more systematic generalization of the qubit example. Instead of the obvious generalization of the diagrams we will focus on constructing appropriate Hilbert spaces for qutrits and other qudits. This will require a use of projectors, which on one hand would limit the growth of the size of the Hilbert space and on the other would produce more connectivity diagrams. Before that let us briefly discuss the cases of two-dimensional and three-dimensional TQFTs.

**Two-dimensional TQFT.** Closed boundaries  $\Sigma$  of two-dimensional manifolds are topological circles  $S^1$ . The cobordisms are realized by smooth two-dimensional surfaces interpolating between boundary circles. If such a surface is oriented it is called a Seifert surface. Every compact oriented surface with non-empty boundary in three dimensions is a Seifert surface of some link (a collection of circles that might be linked) and there are many distinct surfaces for a given link. Consequently, the topology of the surface determines an equivalence class of quantum states.

Local operations correspond to gluing surfaces with only two circular boundaries to a chosen boundary circle. If the glued surface has a non-trivial genus then the topology of the original state will change. However, in this case the operation must be a projector, since there is no smooth topological inverse operation, which reduces the genus. This implies that in a bipartite system represented by a surface of genus  $g$  with two boundaries, the rank of the matrix associated with the state, cannot be smaller than the rank of the matrix of any other surface with the same boundaries, but of genus  $g + 1$  and higher. We have seen that the state with the simply connected topology is expected to have a density matrix of maximal rank, so adding handles should in general reduce the rank. Then a surface of infinite genus

should have the smallest rank, that is to be unentangled (one can understand this as adding too many holes eventually rips up the surface).

The reduction of the rank was illustrated by an explicit computation in the one-dimensional example above and we will not go into further details in two dimensions. As above, one has to take into account that in finite-dimensional TQFTs there are linear relations between states of different genera, as is the case of the first two diagrams in (16). Consequently, there is a finite number of equivalence classes. As a consequence, in finite dimensional TQFTs genus-changing operations may be invertible. Then such operations should control the probability of success in the mutual conversion of states in the same SLOCC class. Invertible local operations with the topology of a sphere are not necessary trivial as such operations can involve (Dehn) twists, changing the complex structure.

One then expects that for a given set of circles, multiple-component Seifert surfaces connecting them correspond to different classes of entanglement, modulo possible linear relations between states. For example, single-component simply connected Seifert surfaces of genus zero should always be maximally entangled, while Seifert surfaces of higher genera, obtained through non-invertible local operators, should in general correspond to subclasses with “weaker” entanglement, characterized by matrices of lower rank. Further details of the correspondence in the two-dimensional case will be studied elsewhere. Here we only comment that the discussion of the one-dimensional case can be embedded in the two-dimensional one if one considers open boundaries. For example, the following diagrams may be considered as the embedding of basis (10) into a two-dimensional TQFT:

$$|e_1\rangle = \begin{array}{c} \text{---} \\ \text{---} \\ \text{---} \end{array} , \quad |e_2\rangle = \begin{array}{c} \text{---} \\ \text{---} \\ \text{---} \end{array} . \quad (18)$$

**Three-dimensional TQFT.** TQFT in three-dimensions are perhaps the most known ones. Chern-Simons theory is a canonical example realizing the TQFT axioms.

In the three-dimensional case we can take  $\Sigma$  to be any closed Riemann surface. The simplest examples are sphere  $\Sigma = S^2$  and torus  $\Sigma = T^2$ . The states are 3-dimensional manifolds filling the space between spheres, tori or more general  $\Sigma$ . Distinct 3D topologies can be classified by the Seifert manifolds – closed 3D manifolds that can be obtained from the states by gluing 3-balls to all open  $S^2$  boundaries, solid tori to all  $T^2$  etc. Seifert manifolds can be obtained from a three-sphere  $S^3$  by cutting out arbitrary number of solid tori, twisting the tori by modular transformations and gluing the twisted tori back – the surgery operation.

As in two dimensions, one can also consider  $\Sigma$  with its own boundaries. The latter can be introduced by removing points from the Riemann surface (introducing punctures). Boundaries of  $\Sigma$  (punctures) extend in three-dimensional bulk as curves, connecting punctures at the boundaries. Another possibility is that such curves do not extend to the boundaries and close in the bulk, producing loops.

In the Chern-Simons theory realization such curves are called Wilson lines. Each such line is characterized by an integrable representations  $R$  of the appropriate Kac-Moody algebra. This is to say that the lines have their own internal attributes. Moreover, representation theory of Kac-Moody algebra induces the property of fusion in lines or TQFT states, which tells that a pair of lines with associated representations  $R_1$  and  $R_2$  are equivalent to a linear combination of lines with representations appearing in the expansion of  $R_1 \otimes R_2$  in irreducible representations.

Wilson lines realize embedding of 1D TQFT in 3D ones, adding importance to the relative position of the lines and endowing some of aspects of one-dimensional theories with a specific mathematical meaning. We can consider the example of level  $k$   $SU(2)$  Chern-Simons theory and  $\Sigma$  being 2-spheres  $S^2$ . Then the fact that the Hilbert space associated with two points is trivial (one-dimensional) can be related to the properties of holomorphic sections of line bundles on the sphere with two punctures [4]. Basis (11) obtained from general considerations in one-dimensional TQFT is related to the basis of conformal blocks in the Wess-Zumino CFT with  $su(2)_k$  Kac-Moody. State (12) is indeed a linear combination of the basis

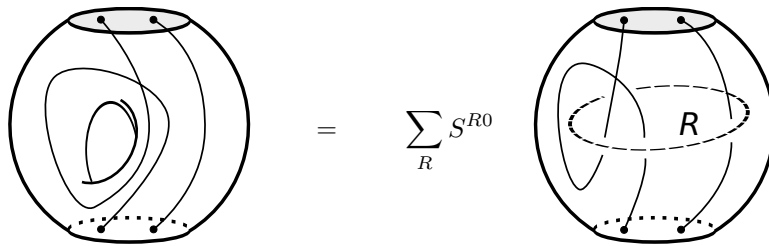


Figure 1: Surgery expresses non-trivial 3D topologies (with “holes”) as linear combinations of simpler ones (with holes filled), but with extra Wilson lines. The diagrams are heuristic depictions of 3-dimensional spaces interpolating between two 2-sphere boundaries.  $S^{R_1 R_2}$  denotes the modular  $S$  transformation in the basis labeled by irreducible representations [4, 37].

states (11) through the following (skein) relations

$$\text{crossing} = A \text{cup} + A^{-1} \text{cap} \quad (19)$$

Parameter  $A$  is expressed in terms of the  $SU(2)$  Chern-Simons data as follows

$$A^{-4} \equiv q = \exp\left(\frac{2\pi i}{k+2}\right). \quad (20)$$

Finally, if a 3D manifold containing a contractible Wilson loop (homeomorphic to a trivial circle) is mapped to a tensor  $T_0$  (scalar, vector, operator etc.) under the TQFT category map, then  $T_0 = \bigcirc T$ , where  $T$  is the image of a manifold without the loop. In other words, unlinked circles can be replaced by numerical factors. In the  $SU(2)$  Chern-Simons TQFT this number is

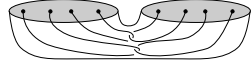
$$\bigcirc \equiv d = -A^2 - A^{-2}. \quad (21)$$

Number  $-d$  is also referred to as “quantum dimension” of the fundamental representation of  $su(2)_k$  Kac-Moody algebra.

Wilson lines and surgeries provide a plethora of realizations of different three-dimensional topologies. Skein relations together with the circle factorization rule allow reducing any knotted topology to a linear combination of topologies with unknotted and unlinked Wilson lines. Similarly, surgeries allow reducing non-trivial three-dimensional topologies of Seifert manifolds to that of  $R^3$  or  $S^3$ . Figure 1 heuristically illustrates how surgery replaces a hole in a 3D topology by a linear combination of spaces without holes but with additional Wilson lines. Therefore, as long as the basis in the Hilbert space is concerned, we can restrict ourselves to a discussion of unknotted and unlinked Wilson lines embedded in a simply-connected 3D topology.

Furthermore, it is sufficient to consider connected topologies due to a property analogous to (14). If a 3-manifold can be cut into two pieces along an  $S^2$  that does not cut any Wilson lines then such a manifold is equivalent to a pair of disconnected 3-manifolds obtained from the original one contracting the  $S^2$  cut to a point. The reason, again, is that  $S^2$  with no punctures corresponds to a trivial Hilbert space. This can be illustrated heuristically by the equivalence of states (4) and (5) up to normalization, if the corresponding diagrams correspond to cobordisms of a pair of  $S^2$ . In other words, disconnected three-dimensional topologies are equivalent to fully connected ones. More generally, the manifolds are truly connected if they cannot be cut into two pieces along an  $S^2$  in such a way that at most two Wilson lines are cut, cf. (14). This has an important consequence for entanglement: one needs Wilson lines to support it if the states are constructed as cobordisms between 2-spheres.

The main purpose of the discussion here, apart from introducing ample set of options in 3D TQFT as compared to the 1D ones, is to show that if we restrict ourselves to manifolds with  $S^2$  boundaries and Wilson lines in the fundamental representation of  $su(2)_k$  the discussion essentially returns to the 1D case with some additional features, such as linear dependence of states with crossings, fusion of lines and the value of  $\bigcirc$ . Let us illustrate the idea by the following example of an entangled state:


(22)

This 3D state can be expanded in the 1D basis via skein relations (19) as follows,


(23)

where each trivial circle  $\bigcirc$  was replaced by factor  $d$ . The state describes two entangled qubits. Using basis (11) one obtains



$$= (A^4 + A^{-4})^2 |00\rangle + (A^4 - A^{-4})^2 |11\rangle$$

$$= 4 \cos^2 \left( \frac{2\pi}{k+2} \right) |00\rangle + 4 \sin^2 \left( \frac{2\pi}{k+2} \right) |11\rangle. \quad (24)$$

This is an entangled state of the Bell SLOCC type, but it is not maximally entangled for  $k \neq 6$  and can only be converted to the maximally entangled one with probability [38] given by

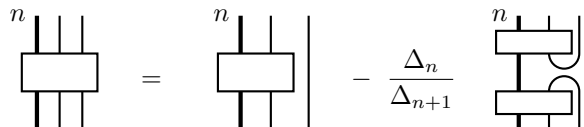
$$p = 2 \min \left\{ \frac{4 \cos^4 \left( \frac{2\pi}{k+2} \right)}{3 + \cos \left( \frac{8\pi}{k+2} \right)}, \frac{4 \sin^4 \left( \frac{2\pi}{k+2} \right)}{3 + \cos \left( \frac{8\pi}{k+2} \right)} \right\}. \quad (25)$$

If we generalize the 1D induced classification of entanglement to this class of states in the 3D TQFT then we will obviously run into the same problem by restricting ourselves only to the diagrams with no crossing or linking. As we have seen, in the 1D case the number of naive diagrams is smaller than the number of the SLOCC classes. Three-dimensional theories give more options, one could include linked Wilson lines and complicated Seifert manifolds in the classification. However, the number of such options is too large, at least in a generic TQFT. They are already redundant in the case of a pair of qubits, as (22) shows. In the next section we will solve the classification mismatch using a connection to representation theory, which will allow us to keep only the crossing-free unlinked diagrams.

## 4 Jones-Wenzl projectors and bipartite entanglement

From now on we understand the ordinary lines in the diagrams as labeled by fundamental representations of  $su(2)_k$ . Diagrams composed of lines can be understood as operators acting on a linear space with the basis provided by diagrams like (10) or their generalizations. In the previous section we gave all the necessary tools to convert the diagrammatic presentation into linear-algebraic form. See also [17, 39].

Jones-Wenzl projectors [30, 31] are useful in the discussion of the diagrammatic presentation of the irreducible representations. For  $su(2)_k$ , operator


(26)

acts as a projector on the maximal spin (symmetric) representation in the tensor product of  $n + 2$  fundamental irreps. Here the thick line with label  $n$  substitutes  $n$  ordinary lines. In (26) the operator is defined recursively and so is  $\Delta_n$ :

$$\Delta_{-1} = 0, \quad \Delta_0 = 1, \quad \Delta_{n+1} = d\Delta_n - \Delta_{n-1}. \quad (27)$$

For example, for two lines corresponding to the fusion rule  $\mathbf{2} \otimes \mathbf{2} = \mathbf{3} \oplus \mathbf{1}$ , the projector on  $\mathbf{3}$  is

$$\begin{array}{c} \text{---} \\ | \\ \text{---} \\ \text{---} \\ | \\ \text{---} \end{array} = \begin{array}{c} | \\ | \\ | \\ | \\ | \\ | \end{array} - \frac{1}{d} \begin{array}{c} \cup \\ \cup \\ \cup \\ \cup \\ \cup \\ \cup \end{array}. \quad (28)$$

The first term in this projector is simply the identity operator, while the second one is the projector on the orthogonal subspace of representation  $\mathbf{1}$ . Note that the  $n$ -line projectors are constructed from the elements of the Temperley-Lieb algebra  $TL_n$ . Projector (28) and the orthogonal projector are equivalent to the basis elements (11).

In another example,  $TL_3$  consists of five elements and the corresponding Jones-Wenzl projector

$$\begin{array}{c} \text{---} \\ | \\ \text{---} \\ \text{---} \\ | \\ \text{---} \end{array} = \begin{array}{c} | \\ | \\ | \\ | \\ | \\ | \end{array} - \frac{d}{d^2-1} \left( \begin{array}{c} \cup \\ \cup \\ \cup \\ \cup \\ \cup \\ \cup \end{array} + \begin{array}{c} \cup \\ \cup \\ \cup \\ \cup \\ \cup \\ \cup \end{array} \right) + \frac{1}{d^2-1} \left( \begin{array}{c} \cup \\ \cup \\ \cup \\ \cup \\ \cup \\ \cup \end{array} + \begin{array}{c} \cup \\ \cup \\ \cup \\ \cup \\ \cup \\ \cup \end{array} \right) \quad (29)$$

projects onto representation  $\mathbf{4}$  in the tensor product  $\mathbf{2} \otimes \mathbf{2} \otimes \mathbf{2}$ . Elements appearing in (29) are the same as in the basis (17).

The Jones-Wenzl projectors have a few useful properties. Their trace-like closure computes the quantum dimension  $(-1)^n \Delta_n$  of the corresponding irrep:

$$\begin{array}{c} n \\ \text{---} \\ | \\ \text{---} \\ \text{---} \\ | \\ \text{---} \end{array} \cup = \Delta_n, \quad \text{in particular,} \quad \begin{array}{c} \text{---} \\ | \\ \text{---} \\ \text{---} \\ | \\ \text{---} \end{array} \cup = \bigcirc \equiv d = \Delta_1. \quad (30)$$

Plat-like closure of the projector (pairwise closure of any pair of input or output lines) nullifies it,

$$\begin{array}{c} \text{---} \\ | \\ \text{---} \\ \text{---} \\ | \\ \text{---} \end{array} \cup \cup = \begin{array}{c} \text{---} \\ | \\ \text{---} \\ \text{---} \\ | \\ \text{---} \end{array} \cup \cup = \begin{array}{c} \text{---} \\ | \\ \text{---} \\ \text{---} \\ | \\ \text{---} \end{array} \cup \cup = 0. \quad (31)$$

We will now use the Jones-Wenzl projectors to construct the Hilbert spaces of qudits. The qutrit space can be built from four  $\mathbf{3}$ -projectors (28). Such space has a basis

$$|e_1\rangle = \begin{array}{c} \bullet \\ \text{---} \\ | \\ \text{---} \\ \text{---} \\ | \\ \text{---} \\ \bullet \end{array} \cup, \quad |e_2\rangle = \begin{array}{c} \bullet \\ \text{---} \\ | \\ \text{---} \\ \text{---} \\ | \\ \text{---} \\ \bullet \end{array} \cup \cup, \quad |e_3\rangle = \begin{array}{c} \bullet \\ \text{---} \\ | \\ \text{---} \\ \text{---} \\ | \\ \text{---} \\ \bullet \end{array} \cup \cup \cup \quad (32)$$

It is not hard to see that these are the only non-null crossing-free options of connecting the projectors allowed by (31) and their number matches the number of irreps in the expansion of  $\mathbf{3} \otimes \mathbf{3} = \mathbf{5} \oplus \mathbf{3} \oplus \mathbf{1}$ . States  $|e_1\rangle$  and  $|e_3\rangle$  are similar to states (10), especially if in the qutrit case one fuses a pair of ordinary lines in one gross line and notices that a single line in (10) is itself a projector on  $\mathbf{2}$ . The fine structure of the gross lines, on the other hand, allows for more connection options.

Again, we can construct an orthonormal basis. For example,

$$|0\rangle = \frac{1}{\Delta_2} |e_1\rangle, \quad |1\rangle = \frac{d}{(\Delta_2 - 1)\sqrt{\Delta_2}} |\hat{e}_2\rangle, \quad |2\rangle = \frac{1}{\sqrt{\Delta_2^2 - \Delta_2 - 1}} (|e_3\rangle - |0\rangle - \sqrt{\Delta_2}|1\rangle) \quad (33)$$

Here, for convenience, we redefined the state  $|e_2\rangle$ :

$$|\hat{e}_2\rangle = |e_2\rangle - \frac{1}{d}|e_1\rangle = \text{Diagram} \quad (34)$$

One can now study possible two-qutrit topologies, that is diagrams connecting eight pairs of points, taking into account local permutations and relations (31). Since there is a larger Hilbert space associated with eight lines, some permutations may act as projectors away from the subspace spanned by basis (33). The valid permutations are only those that do not break the projectors: swapping a pair of projectors, or permutation of lines within the same projector. Similarly, from the point of view of this subspace, there will be several linearly dependent diagrams. A natural choice of linearly independent ones is the following:

$$\begin{array}{ccc} \text{Diagram 1} & , & \text{Diagram 2} & , & \text{and} & \text{Diagram 3} & . \end{array} \quad (35)$$

Using basis (33) one can check that three independent diagrams correspond to matrices of rank one, two and three respectively.

Note that in the above list of diagrams at most four connections between the left and the right subsystems are broken. It is easy to see that breaking more connections would produce operators equivalent to the first diagram, that is a rank one matrix. In other words, one can always consider a half of lines, say the lower four, as unbroken and count the options existing for the other half. In the case of qutrits one ends up with the three options appearing above.

We can now review the case of two qubits. By the same argument the only possible choices are the diagrams

$$\begin{array}{ccc} \text{Diagram 1} & , & \text{and} & \text{Diagram 2} & . \end{array} \quad (36)$$

Now one can generalize this classification to arbitrary qudits, assuming each a state in a Hilbert space of dimension  $d$ . We can describe all the SLOCC classes of entangled pair of qudits  $A$  and  $B$  by diagrams connecting  $4(d - 1)$  pairs of points. One choice of linearly independent diagrams corresponds to those with at least  $2d - 2$  connections between  $A$  and  $B$ , so we can simply classify all the types of entanglement between the qudits by the remaining  $2d - 2$  lines. From these  $2d - 2$  points in either  $A$  or  $B$  only those can be connected by a line that belong to different projectors. Up to permutations within each projector, this approach gives  $d$  independent diagrams, matching the number of SLOCC classes. For

example,  $d = 2, 3, 4$ , one obtains the following *reduced* diagrams

$$d = 2 : \quad \begin{array}{c} \text{---} \cup \text{---} \\ \text{---} \end{array}, \quad \begin{array}{c} \text{---} \\ \text{---} \\ \text{---} \end{array}, \quad (37)$$

$$d = 3 : \quad \begin{array}{c} \text{---} \cup \text{---} \\ \text{---} \cup \text{---} \\ \text{---} \end{array}, \quad \begin{array}{c} \text{---} \\ \text{---} \cup \text{---} \\ \text{---} \end{array}, \quad \begin{array}{c} \text{---} \\ \text{---} \\ \text{---} \\ \text{---} \\ \text{---} \end{array}, \quad (38)$$

$$d = 4 : \quad \begin{array}{c} \text{---} \cup \text{---} \\ \text{---} \cup \text{---} \\ \text{---} \cup \text{---} \\ \text{---} \end{array}, \quad \begin{array}{c} \text{---} \\ \text{---} \cup \text{---} \\ \text{---} \cup \text{---} \\ \text{---} \end{array}, \quad \begin{array}{c} \text{---} \\ \text{---} \\ \text{---} \cup \text{---} \\ \text{---} \cup \text{---} \\ \text{---} \end{array}, \quad \begin{array}{c} \text{---} \\ \text{---} \\ \text{---} \\ \text{---} \\ \text{---} \\ \text{---} \\ \text{---} \end{array}. \quad (39)$$

This classification has a straightforward generalization to the case of qudits of different dimension.

## 5 Tripartite entanglement

In this section we extend the topological classification method to the case of tripartite entanglement. We will focus on the situation with three qubits, for which the classification reduces to drawing all possible connections, with no need of projectors.

In the case of tripartite entanglement between parties  $A$ ,  $B$  and  $C$ , SLOCC classification yields four distinct classes of entanglement [32]. Among the four classes there are the fully separable case (in terms of reduced density matrices of either of subsystems  $A$ ,  $B$  or  $C$  corresponding to  $\text{rk}\rho_A = \text{rk}\rho_B = \text{rk}\rho_C = 1$ ), the partially separable Bell case (only one of  $\rho_A$ ,  $\rho_B$  or  $\rho_C$  having rank one) and two genuinely tripartite classes named GHZ and W. In a general TQFT these characteristic classes should be captured by the following cobordism diagrams:

$$\begin{array}{c} \Sigma_A \\ \text{---} \end{array}, \quad \begin{array}{c} \Sigma_B \\ \text{---} \end{array}, \quad \begin{array}{c} \Sigma_C \\ \text{---} \end{array}, \quad \begin{array}{c} \Sigma_A \cup \Sigma_B \\ \text{---} \end{array}, \quad \begin{array}{c} \Sigma_C \\ \text{---} \end{array}, \quad \begin{array}{c} \Sigma_A \cup \Sigma_B \cup \Sigma_C \\ \text{---} \end{array}. \quad (40)$$

The first two diagrams clearly represent the separable and the Bell case. The last one typically mean the GHZ entanglement, as we will discuss. W class is more intricate. We will only be able to obtain it as a special case of the fully-connected diagram above.

We will focus on 1D TQFT or on 3D TQFT with  $S^2$  boundaries, as explained before. This means that the entanglement will be supported by a skeleton of Wilson lines. The Hilbert space of a qubit is represented by four points (punctures). We will consider states of three qubits up to local permutations of the points.

There are seven nonequivalent ways of connecting the punctures, up to local permutation of points and permutation of parties  $A$ ,  $B$  and  $C$ :

$$\begin{array}{c} \text{UU} \\ \text{---} \end{array}, \quad \begin{array}{c} \text{UU} \\ \text{---} \end{array}, \quad \begin{array}{c} \text{---} \\ \text{---} \cup \text{---} \\ \text{---} \end{array}, \quad \begin{array}{c} \text{---} \\ \text{---} \cup \text{---} \\ \text{---} \end{array}, \quad \begin{array}{c} \text{UU} \\ \text{---} \\ \text{---} \\ \text{---} \end{array}, \quad \begin{array}{c} \text{---} \\ \text{---} \cup \text{---} \\ \text{---} \cup \text{---} \\ \text{---} \end{array}, \quad \begin{array}{c} \text{---} \\ \text{---} \cup \text{---} \\ \text{---} \cup \text{---} \\ \text{---} \end{array}. \quad (41)$$

Since a party connected to the rest of the system by only two lines is not entangled with the rest as (14) suggests (the lines can be cut), we conclude that the diagrams only encode three nonequivalent classes, as the heuristic classification in equation (40). Namely, the first four diagrams describe separable states, the next pair – the Bell type of entanglement, and the last one – a truly tripartite entanglement. The class of the last state can be deduced from explicit evaluation in basis (11). One thus obtains

$$\begin{array}{c} \text{---} \\ \text{---} \cup \text{---} \\ \text{---} \cup \text{---} \\ \text{---} \end{array} = |000\rangle + \frac{1}{\sqrt{d^2 - 1}}|111\rangle, \quad (42)$$

which is a GHZ state.

For completeness we also give the expressions for the remaining diagrams in this basis:

$$\begin{array}{c} \text{UU} \\ \text{---} \\ \text{---} \\ \text{---} \end{array} \begin{array}{c} \text{---} \\ \text{---} \\ \text{---} \end{array} = d^3 |000\rangle, \quad (43)$$

$$\begin{array}{c} \text{UU} \\ \text{---} \\ \text{---} \\ \text{---} \\ \text{---} \end{array} \begin{array}{c} \text{---} \\ \text{---} \\ \text{---} \\ \text{---} \end{array} = d^2 |000\rangle, \quad (44)$$

$$\begin{array}{c} \text{UU} \\ \text{---} \\ \text{---} \\ \text{---} \end{array} \begin{array}{c} \text{---} \\ \text{---} \\ \text{---} \end{array} = d |000\rangle, \quad (45)$$

$$\begin{array}{c} \text{UU} \\ \text{---} \\ \text{---} \\ \text{---} \\ \text{---} \end{array} \begin{array}{c} \text{---} \\ \text{---} \\ \text{---} \\ \text{---} \end{array} = \frac{1}{d^2} \left\{ |000\rangle + (d^2 - 1)^{1/2} (|001\rangle + |010\rangle + |100\rangle) \right. \\ \left. + (d^2 - 1) (|011\rangle + |101\rangle + |110\rangle) + (d^2 - 1)^{3/2} |111\rangle \right\}, \quad (46)$$

$$\begin{array}{c} \text{UU} \\ \text{---} \\ \text{---} \\ \text{---} \\ \text{---} \end{array} \begin{array}{c} \text{---} \\ \text{---} \\ \text{---} \\ \text{---} \end{array} = d (|000\rangle + |011\rangle), \quad (47)$$

$$\begin{array}{c} \text{UU} \\ \text{---} \\ \text{---} \\ \text{---} \\ \text{---} \end{array} \begin{array}{c} \text{---} \\ \text{---} \\ \text{---} \\ \text{---} \end{array} = \frac{1}{d} \left[ |000\rangle + (d^2 - 1)^{1/2} |010\rangle + |101\rangle + (d^2 - 1)^{1/2} |111\rangle \right]. \quad (48)$$

The diagrams are equivalent to unordered 3-vertex graphs with adjacency matrices, with entries in the lines and columns adding up to four. For example,

$$\begin{array}{c} \text{UU} \\ \text{---} \\ \text{---} \end{array} \begin{array}{c} \text{---} \\ \text{---} \end{array} \leftrightarrow \begin{pmatrix} 4 & 0 & 0 \\ 0 & 4 & 0 \\ 0 & 0 & 4 \end{pmatrix}, \quad \begin{array}{c} \text{UU} \\ \text{---} \\ \text{---} \\ \text{---} \end{array} \begin{array}{c} \text{---} \\ \text{---} \\ \text{---} \end{array} \leftrightarrow \begin{pmatrix} 0 & 0 & 4 \\ 0 & 4 & 0 \\ 4 & 0 & 0 \end{pmatrix}, \quad \begin{array}{c} \text{UU} \\ \text{---} \\ \text{---} \\ \text{---} \end{array} \begin{array}{c} \text{---} \\ \text{---} \\ \text{---} \end{array} \leftrightarrow \begin{pmatrix} 0 & 2 & 2 \\ 2 & 0 & 2 \\ 2 & 2 & 0 \end{pmatrix}. \quad (49)$$

This classification misses the W class of SLOCC. Local invertible operations cannot generate the W state from the GHZ state, so the above set of diagrams is insufficient to capture all possible quantum states up to local operations. One possibility is including non-local braiding of the lines. As was mentioned, braiding offers an infinite number of options, so the question is how one can systematically restrict these options to a finite number of classes. In other words, what is the natural diagram for the W state?

Note also that states from W class can be approximated by GHZ-class states with a desired accuracy. In what follows I will present a candidate W state, which is at least an approximation, though no systematic way of constructing such states will be given in this paper.

The W-type entanglement can be detected with a help of 3-tangle  $\tau_{ABC}$  introduced in [40]. It is an entanglement monotone, which means it cannot increase under the action of LOCC. For the GHZ type of entanglement  $\tau_{ABC} > 0$ , with  $\tau_{ABC} = 1$  for the GHZ state. For the W (as well as for the Bell and for the separable) entanglement  $\tau_{ABC} = 0$ . Let us try to design a tripartite entangled state that is not related to GHZ states by a local operator.



than linearly with the number of lines. In TQFT, on the other side, there are natural projectors and subspaces that make the dimension of the Hilbert space grow as needed. Connection with representation theory then ensures that there is a proper match between the classes of diagrams and the classes of entanglement.

The discussion can be generalized to other TQFT as well. The 3D TQFT with sphere boundaries are also examples of 1D TQFT, as explained in the text. One can also consider 3D theories with other type of boundaries. For the case of  $T^2$ , for example, one can adopt the construction of [20] and of the works that followed, where related questions were investigated.

The considered topological classification based on connectivity turns out to be insufficient for higher numbers of parties. In the tripartite case it fails to capture the W state of three qubits. While the W-type states exist in TQFT, it is not clear so far how they are singled out by topology. For four qubits the connectivity classification only finds two non-biseparable classes.

Topology does provide a classification of entangled states, but this classification is too detailed to be practical. The attempt of this paper to restrict it to a finite classification only worked in the bipartite case. Despite this failure the connectivity classification and its possible extensions have a number of advantages. First, it is straightforward to generalize it to an arbitrary number of parties and to arbitrary party dimensions. Most importantly, however, the classification has a very intuitive nature, which tells that to be more entangled, one needs more cables between the parties, while the entanglement distribution depends on how the cables are wired. Even with the current restrictions it may help in designing new quantum states for specific quantum tasks, new measures of entanglements and quantum protocols. For example, an indicator of genuine tripartite entanglement between parties  $A$ ,  $B$  and  $C$  can be constructed from the diagrams representing the state as follows,

$$\tau_3(A) = -\text{Tr}_{\mathcal{H}_A \times \mathcal{H}_A} L \log L, \quad L = \frac{\hat{L}}{\text{Tr}_{\mathcal{H}_A \times \mathcal{H}_A} \hat{L}}, \quad \hat{L} = \begin{array}{c} \begin{array}{ccccccc} & & C & & B & & \\ & & \bullet & & \bullet & & \\ A & \bullet & \text{---} & \bullet & \text{---} & \bullet & A \\ & & \text{---} & & \text{---} & & \\ A & \bullet & \text{---} & \bullet & \text{---} & \bullet & A \\ & & C & & B & & \end{array} \end{array}, \quad (52)$$

where  $\mathcal{H}_A$  is the Hilbert space associated with party  $A$  and the double-line 3-vertex denotes a generic tripartite state of a pure system. The trace should in general be understood as the Markov trace. This ladder, which is made of six such vertices (wavefunctions), can be similarly built for  $B$  and  $C$ , and the result will be non-zero, for either  $\tau_3(A)$ ,  $\tau_3(B)$  or  $\tau_3(C)$ , only if there is three-way entanglement between  $A$ ,  $B$  and  $C$ . The idea here is that the ladder will factorize if any of the chain elements  $A$ ,  $B$  or  $C$  is broken, as in the case of the first two diagrams in (40). Further details and generalizations will be discussed elsewhere.

**Acknowledgments.** I would like to thank João Aires for collaboration at early stages of this project and Rafael Chaves for useful comments. I would also like to thank Gabriel Cardoso, Suresh Nampuri and Roger Picken for the opportunity to present my results at IST Lisbon. This work was supported by RSF grant No. 18-71-10073.

## References

- [1] P. Aravind, *Borromean entanglement of the ghz state*, in *Potentiality, entanglement and passion-at-a-distance*, pp. 53–59. Springer, 1997.
- [2] M. Atiyah, *Topological quantum field theories*, *Inst. Hautes Etudes Sci. Publ. Math.* **68** (1989) 175.
- [3] E. Witten, *Topological Quantum Field Theory*, *Commun. Math. Phys.* **117** (1988) 353.

- [4] E. Witten, *Quantum Field Theory and the Jones Polynomial*, *Commun. Math. Phys.* **121** (1989) 351.
- [5] A. Y. Kitaev, *Fault tolerant quantum computation by anyons*, *Annals Phys.* **303** (2003) 2 [quant-ph/9707021].
- [6] M. H. Freedman, A. Kitaev and Z. Wang, *Simulation of topological field theories by quantum computers*, *Commun. Math. Phys.* **227** (2002) 587 [quant-ph/0001071].
- [7] A. Y. Kitaev, *Unpaired Majorana fermions in quantum wires*, *Phys. Usp.* **44** (2001) 131 [cond-mat/0010440].
- [8] C. Nayak, S. H. Simon, A. Stern, M. Freedman and S. Das Sarma, *Non-Abelian anyons and topological quantum computation*, *Rev. Mod. Phys.* **80** (2008) 1083 [0707.1889].
- [9] L. H. Kauffman, *Quantum computing and the jones polynomial*, *CONTEMPORARY MATHEMATICS* **305** (2002) 101.
- [10] L. H. Kauffman and S. J. Lomonaco Jr, *Entanglement criteria: quantum and topological*, in *Quantum Information and Computation*, vol. 5105, pp. 51–58, International Society for Optics and Photonics, 2003.
- [11] L. H. Kauffman and S. J. Lomonaco Jr, *Braiding operators are universal quantum gates*, *New Journal of Physics* **6** (2004) 134.
- [12] L. H. Kauffman and S. J. Lomonaco Jr, *Quantum knots*, in *Quantum Information and Computation II*, vol. 5436, pp. 268–284, International Society for Optics and Photonics, 2004.
- [13] S. J. Lomonaco and L. H. Kauffman, *Quantum knots and mosaics*, *Quantum Information Processing* **7** (2008) 85.
- [14] D. Melnikov, A. Mironov, S. Mironov, A. Morozov and A. Morozov, *Towards topological quantum computer*, *Nucl. Phys. B* **926** (2018) 491 [1703.00431].
- [15] L. H. Kauffman and E. Mehrotra, *Topological aspects of quantum entanglement*, *Quantum Information Processing* **18** (2019) 1 [1611.08047].
- [16] P. Padmanabhan, F. Sugino and D. Trancanelli, *Quantum entanglement, supersymmetry, and the generalized Yang-Baxter equation*, 1911.02577.
- [17] L. H. Kauffman, *Knot Logic and Topological Quantum Computing with Majorana Fermions*, 1301.6214.
- [18] S. Dong, E. Fradkin, R. G. Leigh and S. Nowling, *Topological Entanglement Entropy in Chern-Simons Theories and Quantum Hall Fluids*, *JHEP* **05** (2008) 016 [0802.3231].
- [19] G. Salton, B. Swingle and M. Walter, *Entanglement from Topology in Chern-Simons Theory*, *Phys. Rev. D* **95** (2017) 105007 [1611.01516].
- [20] V. Balasubramanian, J. R. Fliss, R. G. Leigh and O. Parrikar, *Multi-Boundary Entanglement in Chern-Simons Theory and Link Invariants*, *JHEP* **04** (2017) 061 [1611.05460].
- [21] S. Chun and N. Bao, *Entanglement entropy from  $SU(2)$  Chern-Simons theory and symmetric webs*, 1707.03525.

- [22] S. Dwivedi, V. K. Singh, S. Dhara, P. Ramadevi, Y. Zhou and L. K. Joshi, *Entanglement on linked boundaries in Chern-Simons theory with generic gauge groups*, *JHEP* **02** (2018) 163 [1711.06474].
- [23] V. Balasubramanian, M. DeCross, J. Fliss, A. Kar, R. G. Leigh and O. Parrikar, *Entanglement Entropy and the Colored Jones Polynomial*, *JHEP* **05** (2018) 038 [1801.01131].
- [24] D. Melnikov, A. Mironov, S. Mironov, A. Morozov and A. Morozov, *From Topological to Quantum Entanglement*, *JHEP* **05** (2019) 116 [1809.04574].
- [25] G. M. Quinta and R. André, *Classifying quantum entanglement through topological links*, *Phys. Rev. A* **97** (2018) 042307 [1803.08935].
- [26] S. Dwivedi, V. K. Singh, P. Ramadevi, Y. Zhou and S. Dhara, *Entanglement on multiple  $S^2$  boundaries in Chern-Simons theory*, *JHEP* **08** (2019) 034 [1906.11489].
- [27] S. Dwivedi, A. Addazi, Y. Zhou and P. Sharma, *Multi-boundary entanglement in Chern-Simons theory with finite gauge groups*, *JHEP* **04** (2020) 158 [2003.01404].
- [28] N. Bao, N. Cheng, S. Hernández-Cuenca and V. P. Su, *Topological Link Models of Multipartite Entanglement*, *Quantum* **6** (2022) 741 [2109.01150].
- [29] M. Buican and R. Radhakrishnan, *Galois orbits of TQFTs: symmetries and unitarity*, *JHEP* **01** (2022) 004 [2109.02766].
- [30] V. F. R. Jones, *A polynomial invariant for knots via von Neumann algebras*, *Bull. Am. Math. Soc.* **12** (1985) 103.
- [31] H. Wenzl, *On sequences of projections*, *CR Math. Rep. Acad. Sci. Canada* **9** (1987) 5.
- [32] W. Dur, G. Vidal and J. I. Cirac, *Three qubits can be entangled in two inequivalent ways*, *Phys. Rev. A* **62** (2000) 062314 [quant-ph/0005115].
- [33] F. Verstraete, J. Dehaene, B. De Moor and H. Verschelde, *Four qubits can be entangled in nine different ways*, *Physical Review A* **65** (2002) 052112.
- [34] R. Horodecki, P. Horodecki, M. Horodecki and K. Horodecki, *Quantum entanglement*, *Rev. Mod. Phys.* **81** (2009) 865 [quant-ph/0702225].
- [35] M. Walter, B. Doran, D. Gross and M. Christandl, *Entanglement polytopes: multiparticle entanglement from single-particle information*, *Science* **340** (2013) 1205.
- [36] D. Melnikov, *Topological View on Entanglement and Complexity*, *Springer Proc. Phys.* **239** (2020) 271.
- [37] E. P. Verlinde, *Fusion Rules and Modular Transformations in 2D Conformal Field Theory*, *Nucl. Phys. B* **300** (1988) 360.
- [38] G. Vidal, *Entanglement of pure states for a single copy*, *Phys. Rev. Lett.* **83** (1999) 1046 [quant-ph/9902033].
- [39] L. H. Kauffman, S. L. Lins and S. Lins, *Temperley-Lieb recoupling theory and invariants of 3-manifolds*, no. 134. Princeton University Press, 1994.
- [40] V. Coffman, J. Kundu and W. K. Wootters, *Distributed entanglement*, *Phys. Rev. A* **61** (2000) 052306 [quant-ph/9907047].